ACS Catalysis

RESEARCH ARTICLE

pubs.acs.org/acscatalysis

Structural Changes of γ-Al_2O_3-Supported Catalysts in Hot Liquid Water

Ryan M. Ravenelle,[†] John R. Copeland,[†] Wun-Gwi Kim,[†] John C. Crittenden,[‡] and Carsten Sievers[†,*]

[†]School of Chemical & Biomolecular Engineering, Georgia Institute of Technology, 311 Ferst Drive NW, Atlanta, Georgia 30332, United States

[‡]Brook Byers Institute for Sustainable Systems and School of Civil & Environmental Engineering, Georgia Institute of Technology, 800 West Peachtree Street NW, Atlanta, Georgia 30332, United States

Supporting Information

ABSTRACT: The structural changes of γ-Al_2O_3, Ni/γ-Al_2O_3, and Pt/γ-Al_2O_3 catalysts under aqueous phase reforming conditions (liquid water at 200 °C and autogenic pressure) are examined over the course of 10 h. The changes are characterized by X-ray diffraction, NMR spectroscopy, N_2 physisorption, pyridine adsorption followed by IR spectroscopy, and electron microscopy. It is demonstrated that γ-alumina is converted into a hydrated boehmite (AlOOH) phase with significantly decreased acidity and surface area. For metal-free γ-alumina, the transformation is completed within 10 h, whereas the presence of nickel and platinum particles significantly retards the formation of boehmite. In the beginning of the treatment, the surface area of γ-alumina increases, suggesting surface pitting and formation of small boehmite particles on the surface of γ-alumina. This process is followed by the formation of a compact crystalline boehmite phase. It is proposed that the metal particles affect the kinetics of this transformation by blocking specific surface hydroxyl groups that act as initial hydration sites. The transformation of γ-alumina into boehmite is accompanied by sintering of the supported metal particles.

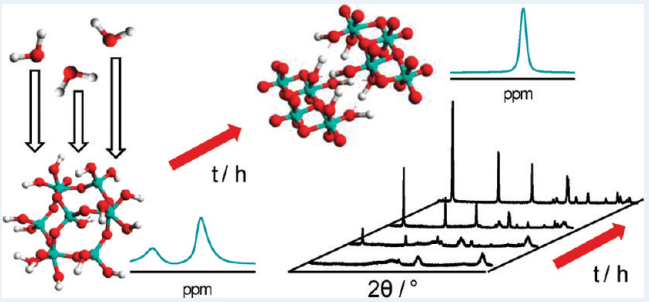

KEYWORDS: alumina, catalysis, biomass, hydrothermal stability, aqueous phase reforming, hydration

1. INTRODUCTION

Heterogeneously catalyzed conversion of biomass will likely play an important role in transitioning to renewable feedstock-based fuels and chemicals. Such processes will enable biorefineries to compete with traditional fossil-fuel-based refineries, which employ a variety of heterogeneously catalyzed processes, such as fluid catalytic cracking. Many components found in biomass feedstocks have very low vapor pressures, and sugars and sugar alcohols tend to degrade at temperatures lower than their boiling points.[1] Therefore, processes for conversion of carbohydrates will likely take place in liquid phase. In light of this issue, a recent NSF report concluded that improving liquid-phase processes for biomass-derived compounds is necessary to enable large scale production.[2] Water is the likely solvent of choice because it is cheap, abundant, and readily dissolves polar oxygenates from biomass, including monosaccharides, some oligomeric species, and sugar alcohols (e.g., xylitol, sorbitol). The use of aqueous media imposes new requirements on the stability of heterogeneous catalysts that were typically designed for use in gas phase reaction. However, only a few publications have addressed the stability of solid catalysts and supports under conditions that are relevant for biomass reforming.[3,4] A recent US-DOE report identified the need for catalysts that are stable under aqueous phase reforming conditions as one of the key challenges for the development of economical processes for biofuel production.[5]

Transition and noble metals supported on metal oxide supports have shown potential for catalytic upgrading of biomass-derived feedstocks in aqueous phase.[6−8] Specifically, γ-Al_2O_3 supported catalysts have been used for aqueous phase reforming of biomass-derived oxygenates as well as hydrolysis/hydrogenation of microcrystalline cellulose to sugar alcohols.[9−11] Although these publications clearly demonstrated the activity and selectivity of supported metal catalysts in water, they did not address their stability under reforming conditions (e.g., 150 °C < T < 265 °C, $P^*_{H_2O}(T) < P <$ 100 bar).

It is well established that γ-Al_2O_3 will rehydrate in the presence of water and that boehmite (AlOOH) is thermodynamically favored over gibbsite above 150 °C.[12,13] This transformation was also observed for supported metal catalysts; namely, 0.9 wt % Pt/γ-Al_2O_3 used for glycerol reforming at 220 °C and 2.50 MPa over 14 h,[14] as well as for Ru/Al_2O_3 treated with H_2-saturated water at 200 °C and 40 atm over 5 h.[15] However, the design of novel catalysts or regeneration procedures depends on an improved understanding of the kinetics of these phase

Received: December 22, 2010
Revised: March 22, 2011
Published: April 08, 2011

transitions and insight into how these changes affect the properties of the catalyst (e.g., surface acidity).

In this article, we elucidate structural transformations as well as changes in acid site concentration and metal dispersion of 1 wt % Pt/γ-Al_2O_3 and 1 wt % Ni/ γ-Al_2O_3 supported catalysts under conditions that are relevant for biomass reforming (i.e., liquid water at 200 °C and $P^*_{H_2O}$) as a function of treatment time. In addition, we investigate the kinetics of boehmite formation and the effect of metal particles on this transition as well as the importance of specific surface hydroxyl groups for alumina hydration.

2. EXPERIMENTAL SECTION

Catalyst Preparation. The catalysts were prepared via an incipient wetness procedure, which consists in dissolving the required mass of metal precursor in the minimum amount of water needed to fill the pore of the dried support. The slurry was mechanically stirred to achieve maximum homogeneity during the addition of water. The metal precursors were $H_2PtCl_6 \cdot 6H_2O$ (ACS reagent grade, Sigma Aldrich) and $Ni(NO_3)_2 \cdot 6H_2O$ (99.999% metals basis, Aldrich), and the support was γ-Al_2O_3 (3 μm APS powder, 99.97% metals basis, Alfa Aesar). The catalysts were then calcined in air at 500 °C (ramp 1 K·min^{-1}) for 4 h, followed by reduction in 10% H_2/He at 300 °C (ramp 5 K·min^{-1}) for 3 h prior to treatment.

Catalyst Treatment. Catalyst treatments were performed in a manner similar to methods found elsewhere.[3] Briefly, 0.5 g of the solid was suspended in 30 mL of deionized water. Each mixture was poured into an autoclave with a Teflon liner, which was placed in a preheated oven at 200 °C under constant agitation. After a specific amount of time, the reaction was quenched by placing the autoclave in an ice bath. The mixture was filtered (0.45 μm Nylon filter), and the solids were dried in air prior to characterization.

X-ray Diffraction. Powder X-ray diffraction (XRD) patterns were measured on a Philips X'pert diffractometer equipped with an X'celerator module using Cu Kα radiation. Diffractograms were obtained from $2\theta = 5-70°$ with a step size of 0.0167°.

NMR Spectroscopy. ^{27}Al MAS NMR measurements were performed on a Bruker DSC 400 spectrometer. The samples were packed into a 4 mm zirconia rotor and spun at 12 kHz. The resonance frequency for ^{27}Al was 104.2 MHz. A $\pi/12$ pulse was used for excitation, and the recycling delay was 250 ms. For each spectrum, a minimum of 2400 scans were accumulated. Solid $Al(NO_3)_3$ was used as a reference compound ($\delta = -0.543$ ppm). To calculate the boehmite fraction, the normalized ^{27}Al spectra were fitted as a linear combination of the spectra of pure boehmite and pure alumina.

^{1}H MAS NMR measurements were performed on the same instrument with adamantane as a reference compound ($\delta = 1.756$ ppm). Prior to analysis, the samples were dried under vacuum at 200 °C overnight and packed into 4 mm zirconia rotors in a drybox. Samples were spun at 12 kHz for a total number of 64 scans. The obtained spectra were normalized by the sample mass and fitted with Lorentzian peaks. The reference spectrum of adamantane was also used as an external standard for determining the concentration of hydroxyl groups in the samples.

Pyridine Adsorption Followed by IR Spectroscopy. IR spectra of adsorbed pyridine were collected on a Nicolet 8700 FT-IR spectrometer with a MCTA detector using 64 scans per spectrum and a resolution 1 cm^{-1}. Each catalyst material was pressed into a self-supported wafer and loaded into a custom-built vacuum chamber with Teflon-sealed ZnSe windows.

The self-supported wafers were first activated at ~10^{-6} mbar and 200 °C for 1 h. The temperature was then decreased to 150 °C, and pyridine was dosed into the chamber with at a pressure of 0.1 mbar. After evacuation for at least 30 min, the relevant peaks were integrated. The density of the wafer was obtained by weighing a disk with a diameter of 3.2 mm that was punched out of the wafer after the experiment. The concentration of acid sites was calculated on the basis of the integral of the peaks, the density of the wafer, and the molar extinction coefficients reported by Datka et al.[16]

Nitrogen Physisorption. Physisorption measurements were performed on a Quantachrome Quadrasorb SI surface area and pore volume analyzer at the temperature of liquid nitrogen (−196 °C). Prior to analysis, samples were degassed at 200 °C for two hours under vacuum. The surface area was calculated using the multipoint BET method from the adsorption isotherm in the relative pressure range $0.05 \leq P/P_0 \leq 0.3$.

H_2−O_2 Titration. Hydrogen chemisorptions experiments were performed on a Micromeritics AutoChem II Chemisorption Analyzer equipped with a thermal conductivity detector. The samples were first treated at 200 °C for 1 h with argon as carrier gas to eliminate adsorbed water. The sample was then cooled to room temperature, after which it was ramped to 300 °C (5 K/min) under 10% H_2/Ar. After reduction, the sample was brought to 40 °C, and 20 pulses of 4% H_2/Ar were admitted, followed by dosing with 10% O_2/He. A final dosing of 4% H_2/Ar was performed and used for the dispersion analysis. A H_2/Pt surface stoichiometry of 1.5 was assumed according to the proposed reactions during titration.[17,18]

$$Pt + (1/2)H_2 \rightarrow Pt - H \quad (1)$$

$$Pt + (1/2)O_2 \rightarrow Pt - O \quad (2)$$

$$Pt - O + (3/2)H_2 \rightarrow Pt - H + H_2O \quad (3)$$

SEM and TEM. Field emission scanning electron microscopy (FE-SEM) images were obtained on a JEOL LEO-1530 at a landing energy of 10 kV. The sample powder was spread on a carbon-coated sample mount and gold-coated to prevent surface charging effects. Optimum images were taken with the "in lens" detector mode and 9 mm of working distance.

Field emission transmission electron microscopy (FE-TEM) images were taken with a Hitachi HF-2000 at 200 kV accelerating voltage. The powder samples were first dispersed in water by sonication. A few drops of sample solution were placed on a carbon-coated TEM grid (lacey), followed by drying in an oven at 80 °C. The optimum images were taken at the lowest contrast condition in the middle of overfocusing and under-focusing conditions.

3. RESULTS

3.1. XRD. Untreated γ-alumina shows the expected diffraction pattern characteristic of the defective spinel structure with the two main peaks located at $2\theta = 45.8°$ and 67° corresponding to the (400) and (440) crystal planes, respectively (Figure 1).[19] The formation of small peaks from a crystalline phase is observable

dx.doi.org/10.1021/cs1001515 |ACS Catal. 2011, 1, 552–561

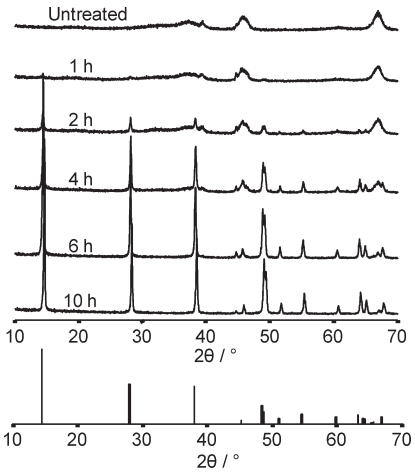

Figure 1. X-ray diffractograms of γ-Al_2O_3 treated at 200 °C and vapor pressure for various durations.

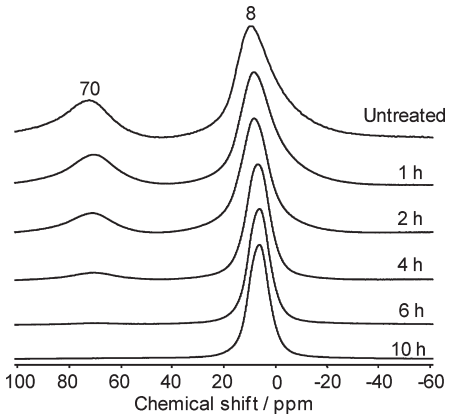

Figure 2. ^{27}Al NMR spectra of γ-Al_2O_3 treated at 200 °C and vapor pressure for various durations.

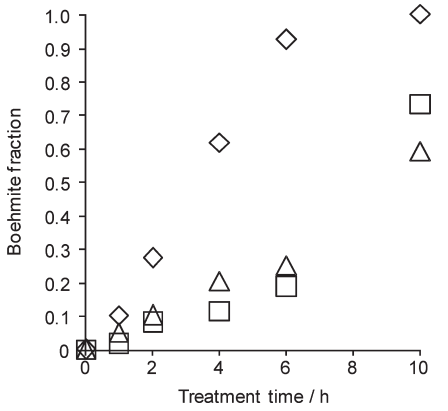

Figure 3. Kinetics of boehmite formation during treatment in liquid water at 200 °C: ◇ = γ-Al_2O_3, △ = 1 wt % Pt/γ-Al_2O_3, □ = 1 wt % Ni/γ-Al_2O_3.

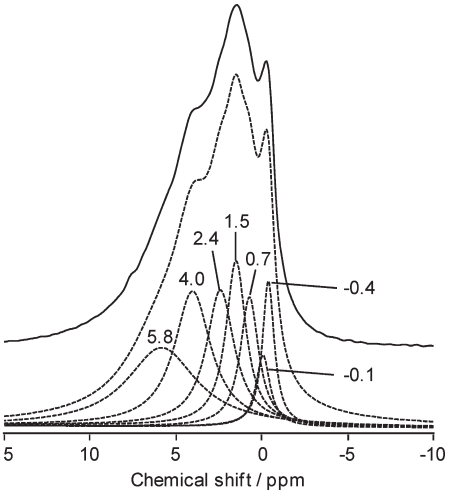

Figure 4. Normalized ^{1}H NMR spectra of untreated γ-Al_2O_3 (solid line) and peak deconvolution (dashed lines).

within the first hour of the treatment. These peaks increased in intensity with increasing treatment time. The crystal phase was identified as boehmite through comparison to a standard reference diffractogram with the main peaks located at 2θ = 14.5°, 28.2°, 38.3°, 49°, and 49.3° corresponding to the (020), (120), (140 and 031), (051), and (200) crystal planes, respectively (Figure 1).[19,20]

The X-ray diffractograms of the untreated supported metal catalysts did not exhibit distinct peaks corresponding to metal particles due to the their small size. Comparison of the X-ray diffractograms of bare γ-Al_2O_3 with the supported metal catalysts indicates that the crystallization occurs more slowly when metal particles are present (Supporting Information, Figure S1). After 10 h of treatment, Ni/γ-Al_2O_3 has more intense refraction of the main peaks at 2θ = 14.5°, 28.2°, and 38.3° compared with Pt/γ-Al_2O_3. The platinum-loaded catalyst also shows evidence of the (400) crystal plane of γ-Al_2O_3 at 2θ = 45.8°.[19]

3.2. ^{27}Al MAS NMR Spectroscopy. The ^{27}Al MAS NMR spectra of the untreated samples contain resonances at 8 and 70 ppm, which are attributed to octahedrally and tetrahedrally coordinated aluminum species, respectively (Figures 2 and S2).[21,22]

This shows the expected distribution of Al nuclei between two different positions in γ-alumina.[12] Untreated γ-Al_2O_3 contained 28% of aluminum in tetrahedral coordination (Al_T), consistent with previous investigations.[23,24] In contrast, all aluminum atoms in boehmite are octahedrally coordinated.[22] The fraction of Al present as boehmite in each sample was determined by linear combination of the ^{27}Al MAS NMR spectra of γ-Al_2O_3 and boehmite (Figure 3). The validity of this approach was confirmed by thermogravimetric analysis (Figure S4, Table S1 of the Supporting Information). The results from both methods were in good agreement. Therefore, it is concluded that the samples do not contain "NMR-invisible aluminum", which might be found in penta-coordinated and heavily distorted environments.

γ-Alumina was essentially completely converted to boehmite within 6 h at an initial rate of 0.10 mol fraction·h^{-1}. For the metal loaded samples, the Al_T resonance was observable over longer treatment times than for the bare support (Figures 3 and S2). The metal loaded samples form boehmite particularly slowly during the first 6 h, with initial rates of 0.05 and 0.02 mol fraction·h^{-1} for Pt/γ-Al_2O_3 and Ni/γ-Al_2O_3, respectively. After 6 h of treatment, the rates increased to 0.086 and 0.136 mol fraction·h^{-1} for Pt/γ-Al_2O_3 and Ni/γ-Al_2O_3, respectively. It is interesting to note that the kinetics of the phase transition were similar for both catalyst materials, with 73% conversion for Ni/γ-Al_2O_3 after 10 h compared with 60% for Pt/γ-Al_2O_3.

dx.doi.org/10.1021/cs1001515 |*ACS Catal.* 2011, 1, 552–561

Table 1. Hydroxyl Coverage of Untreated Materials As Measured by ^{1}H MAS NMR Spectroscopy

	γ-Al_2O_3	1 wt % Ni/γ-Al_2O_3		1 wt % Pt/γ-Al_2O_3	
	C_{OH}/mmol·g^{-1}	C_{OH}/mmol·g^{-1}	Δ/%	C_{OH}/mmol·g^{-1}	Δ/%
δ = 2.4 ppm 3Al(OH)	0.27	0.20	−25	0.25	−8
δ = 1.5 ppm 2Al(OH)	0.24	0.15	−39	0.25	6
δ = 0.7 ppm 2Al(OH)	0.17	0.12	−28	0.17	0.0
δ = −0.1 ppm Al(OH)	0.07	0.04	−39	0.08	8
δ = −0.4 ppm Al(OH)	0.13	0.08	−35	0.06	−53

3.3. ^{1}H MAS NMR Spectroscopy. The ^{1}H NMR spectra of γ-Al_2O_3 showed six peaks located at 5.8, 4.0, 2.4, 1.5, 0.7, −0.1, and −0.4 ppm (Figure 4). The peaks at 5.8 and 4.0 ppm are attributed to adsorbed water, leaving 5 OH surface species.[25] The high field signals at −0.4 and −0.1 ppm indicate hydroxyl groups attached to a single Al atom, whereas the resonances at 0.7 and 1.5 ppm are attributed to Al−OH−Al species, and the peak at 2.4 ppm is assigned to an OH coordinated to three Al atoms.[25] This is consistent with the surface model of γ-Al_2O_3 proposed by Knözinger and Ratnasamy, which postulates five types of possible surface hydroxyl groups, three of which involve oxygen bridging neighboring aluminum atoms (Al_T−OH−Al_O, Al_O−OH−Al_O, and $3Al_O$−OH).[26]

The OH group density of untreated γ-Al_2O_3 is calculated to be 0.89 mmol·g^{-1}, or 5.9 OH groups·nm^{-2}, excluding resonances from water (Table 1). This value is slightly lower than other ^{1}H NMR investigations of dehydrated γ-alumina that have shown a hydroxyl group density of 8.5 OH·nm^{-2}.[27] It should also be noted that different γ-alumina samples will have different hydroxyl group densities, depending on their structure.

A comparison of the ^{1}H NMR spectra of untreated γ-alumina and the catalysts demonstrated a change in the hydroxyl group concentration upon addition of metal (Figure S3, Table 1). Ni/γ-Al_2O_3 showed decreases in all hydroxyl group concentrations in the range of 25−39% with slightly larger decreases of the resonances corresponding to OH groups bound to a single Al atom. The platinum catalyst showed the most significant decrease in the singly coordinated OH group resonating at −0.4 ppm, with a 53% decrease in concentration. The concentrations of the other hydroxyl groups did not change appreciably.

3.4. Pyridine Adsorption, Followed by IR Spectroscopy. The acidity of treated and untreated γ-Al_2O_3 samples was analyzed by pyridine adsorption, followed by IR spectroscopy, as described elsewhere.[16,28,29] The absence of a band at 1540 cm^{-1} indicated that there are no Brønsted acid sites capable of protonating pyridine on untreated γ-alumina or any of the other samples.[16,30] A Lewis acid site (LAS) concentration of 342 μmol·g^{-1} was determined for untreated γ-Al_2O_3 on the basis of the intensity of the characteristic band at 1451 cm^{-1} (Figure 5). A notable decrease of the LAS concentration from 304 to 42 μmol·g^{-1} was observed between 2 and 6 h of treatment time.

The LAS concentration of untreated Ni/γ-Al_2O_3 was lower than that of alumina at 262 μmol·g^{-1}. It decreased to 216 and 140 μmol·g^{-1} after 6 and 10 h of treatment, respectively. The latter concentration corresponds to a 53% decrease compared with the untreated material. The untreated Pt/γ-Al_2O_3 catalyst had a LAS concentration of 441 μmol·g^{-}1, which is higher than that of untreated γ-alumina. After 6 h of treatment, the LAS concentration dropped to a value of 243 μmol·g^{-1}, and after 10 h treatment, 189 μmol·g^{-1} sites remained, 43% of the initial

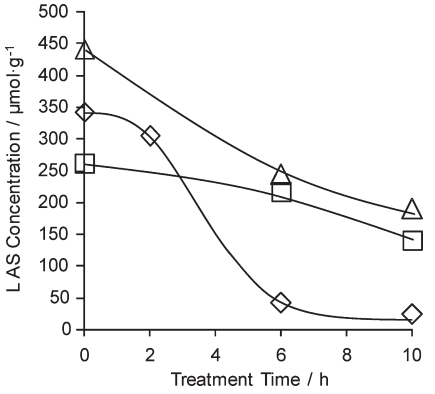

Figure 5. Change in Lewis acid site (LAS) concentration as a function of treatment time as measured by adsorbed pyridine: ◊ = γ-Al_2O_3, Δ = 1 wt % Pt/γ-Al_2O_3, □ = 1 wt % Ni/γ-Al_2O_3.

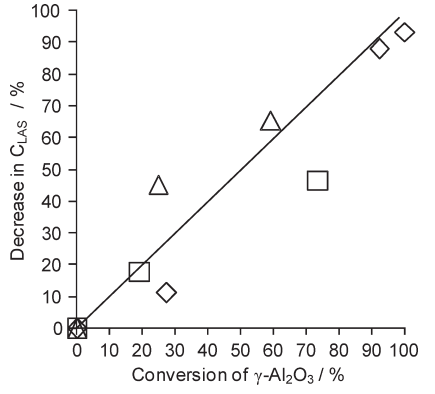

Figure 6. Decrease in Lewis acid site (LAS) concentration as a function of support conversion: ◊ = γ-Al_2O_3, Δ = 1 wt % Pt/γ-Al_2O_3, □ = 1 wt % Ni/γ-Al_2O_3.

value. The decrease in the LAS concentration of both metal catalysts was gradual compared with γ-alumina. The relative decrease in LAS concentration correlated linearly with the increase in the conversion of γ-alumina to boehmite (Figure 6).

3.5. Nitrogen Physisorption. Untreated γ-Al_2O_3 had a BET surface area of ∼90 m^2·g^{-1}, whereas the surface area of both metal containing samples was ∼70 m^2·g^{-1} (Figure 7). Initially, hydrothermal treatment led to an increase in the surface area. For metal-free γ-Al_2O_3, a maximum of 104 m^2·g^{-1} was observed after 2 h, followed by a sharp decline to 32 m^2·g^{-1} after 6 h.

In contrast, the surface area of both supported metal catalysts increased for the first 6 h of treatment and decreased less sharply when the treatment time was extended. Note that the platinum

dx.doi.org/10.1021/cs1001515 |ACS Catal. 2011, 1, 552–561

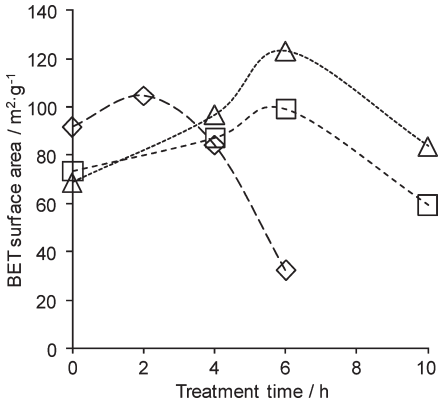

Figure 7. Changes in catalyst surface area relative to treatment time as measured by N_2 physisorption. (◊ = γ-Al_2O_3, Δ = Pt/γ-Al_2O_3, □ = Ni/γ-Al_2O_3).

catalyst after 10 h of treatment had a higher surface area (84 $m^2 \cdot g^{-1}$) than the untreated sample (69 $m^2 \cdot g^{-1}$), whereas the nickel catalyst had a surface area of 59 $m^2 \cdot g^{-1}$ after 10 h compared with 73 $m^2 \cdot g^{-1}$ for the untreated material. Although N_2 physisorption may potentially underestimate surface areas of poorly crystalline boehmite,[31] it provides a common qualitative indicator of surface areas.

3.6. H_2/O_2 Titration. A slight increase in the Pt dispersion was observed over the first 4 h, whereas the dispersion was reduced to 21% after 10 h of treatment (Table 2). Ni/Al_2O_3 samples were not analyzed because it is difficult to obtain reliable estimation of Ni dispersions at low loadings (i.e., <3 wt %) due to strong metal−support interactions.[32]

3.7. Electron Microscopy. TEM images of both untreated Pt/γ-Al_2O_3 and Ni/γ-Al_2O_3 indicate metal particle sizes between 0.5 and 2.0 nm, with average sizes of 1.0 and 1.2 nm, respectively (Figure 8). The metal particles remained in the size range between 0.5 and 2.0 nm after 4 h of treatment for Pt/γ-Al_2O_3 and Ni/γ-Al_2O_3 (Figure 9). After 10 h, the particle size distribution shifted to larger particles for both samples. Specifically, 12% of Pt particles and 16% of the Ni particles exceeded 2 nm, whereas average metal particle sizes were 1.7 and 1.6 nm for Pt/γ-Al_2O_3 and Ni/γ-Al_2O_3, respectively. Pt particles as large as 8 nm were observed in addition to enhanced contrast (Figure S5). For Ni/γ-Al_2O_3, the contrast between nickel particles and alumina pore structure was less pronounced, as has been observed by others with such low nickel loading.[33] This may be due to the presence of unreduced NiO particles, which have extinction distances similar to those of the the γ-Al_2O_3 (400) plane, making contrast resolution more difficult.[18]

SEM images of the Pt/γ-Al_2O_3 samples show that the alumina particles tend to agglomerate and form compact structures over the course of treatment (Figure 10). The untreated Pt/Al_2O_3 had some large observable particles up to ∼450 nm in size, whereas most were in the range of 100 nm or less. After 4 h of treatment, particles larger than 1100 nm were observed with many smaller clusters ∼200 nm in diameter. At the same time, the surface roughness decreased markedly.

4. DISCUSSION

4.1. Stability of γ-Alumina in Hot Liquid Water. Because γ-Al_2O_3 is prepared from the dehydration of gibbsite mineral,[12]

Table 2. Summary of Metal Particle Characteristics for Untreated Platinum Catalyst and Samples Treated for 4 and 10 h at 200 °C and Saturation Pressure

catalyst	dispersion/%	metallic surface area/$m^2 \cdot g^{-1}$	active particle diameter/nm
Pt/γ-Al_2O_3, untreated	70.2	1.73	1.61
Pt/γ-Al_2O_3, treated 4 h	78.4	1.94	1.45
Pt/γ-Al_2O_3, treated 10 h	21.2	0.523	5.35

$Al(OH)_3$, it is not surprising that under hydrothermal treatment, it reverts to a hydrated form. The phase changes of aluminum oxides and hydroxides under steaming conditions are dependent on a number of factors, including particle size, concentration of steam, and heating rate (Scheme 1).[34,35]

The thermodynamic stability of different phases in liquid water depends on the temperature, pH, and potential of the solution.[13] However, these transformations have been overlooked in a considerable number of publications, particularly in studies utilizing alumina supported catalysts for conversion of biomass in water at elevated temperatures. This may be a critical oversight, as the alumina phase can have a significant impact on activity. For example, platinum supported on a mixed phase alumina support leads to a ∼6-fold increase in the hydrogen production rate from aqueous phase reforming of glycerol compared with platinum supported on γ-alumina alone.[36] Therefore, the stability of metal oxide supports, and γ-Al_2O_3 in particular, must be an important consideration in the development of heterogeneous catalysts.

Hydration of alumina at room temperature is a process that can take weeks for appreciable conversion, and both pH and calcination conditions can influence which phase is formed.[37,38] One study even reported on hydration of alumina at room temperature over the course of 6 months with bayerite as the main product.[39] The formation of boehmite from γ-Al_2O_3 synthesized by the sol−gel method was reported after this material was treated at 200 °C in liquid water under autogenous pressure for several days.[40] The current study shows that γ-Al_2O_3-based catalysts undergo significant transformations on much shorter time scales.

Reaction kinetics based on quantitative analysis of ^{27}Al MAS NMR spectra showed that the concentration of boehmite formed from the bare γ-alumina support increased linearly over the course of the first 6 h, after which 92% of the material had been converted (Figure 3). It is important to note that the XRD peaks after 1 and 2 h of treatment were rather low in intensity (Figure 1), although the NMR spectra indicated that a considerable number of the Al nuclei were already hydrated (Figure 3). These observations demonstrate the lack of long-range order in the hydrated alumina phases in these samples. The formation of first hydrated alumina phases was accompanied by a 14% increase in the surface area. This observation is tentatively assigned to the formation of small patches of boehmite that are attached to the alumina surface. Pitting of the alumina phase due to migration of Al atoms to the boehmite patches may also contribute to the increase in surface area. After 2 h, a decrease in the surface area accompanied by a notable increase in the intensity of the XRD peaks indicated the formation of a compact crystalline boehmite phase. The formation of compact particles was also observed in the SEM images (Figure 10). Note that an initial increase in the

dx.doi.org/10.1021/cs1001515 |ACS Catal. 2011, 1, 552–561

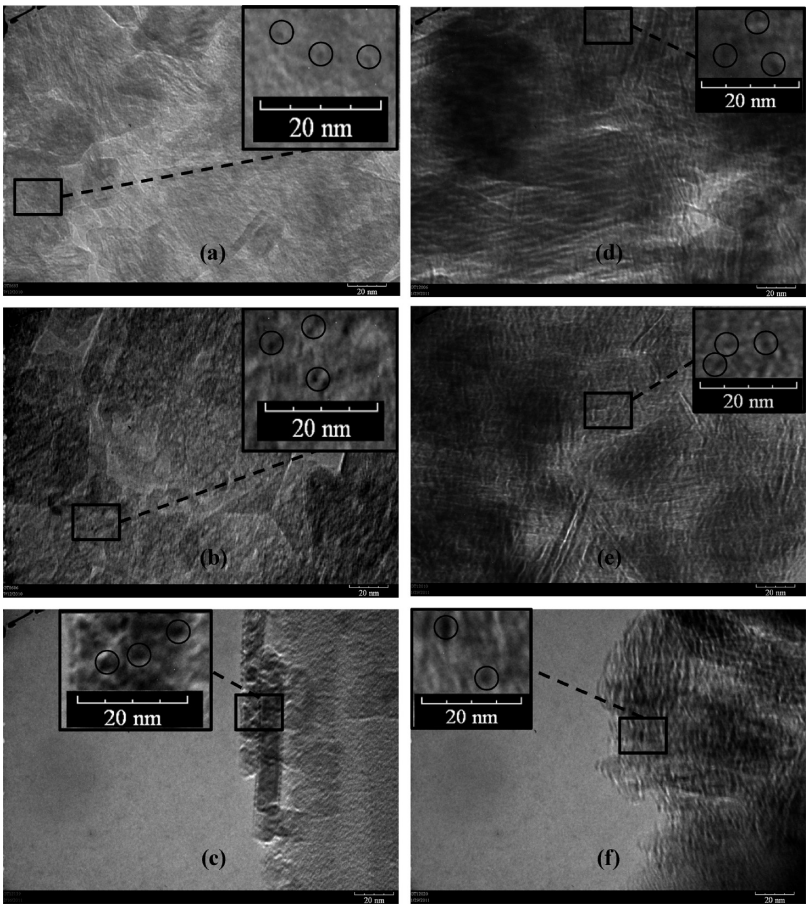

Figure 8. TEM analysis of 1 wt % Pt/γ-Al_2O_3 untreated (a), treated for 4 h (b), and treated for 10 h (c) and 1 wt % Ni/γ-Al_2O_3 untreated (d), treated for 4 h (e), and treated for 10 h (f) at 200 °C and vapor pressure.

surface area followed by an eventual decrease was also observed for the phase transformation of gibbsite crystals to boehmite in water vapor.[41] The authors suggested a mechanism including dissolution of aluminum atoms from nonequilibrium phase, followed by nucleation and growth of stable boehmite (AlOOH) crystals.

4.2. Effect of Metal Particles on Boehmite Formation. Although the formation of boehmite has been reported for supported metal catalysts before,[14,15] the effect of metal particles on the kinetics of boehmite formation on this time scale have not been investigated in detail. A recent study on 17 wt % Ni/γ-Al_2O_3 in the temperature range of 90−150 °C over the course of 48 h concluded that the nickel particles did not affect the hydration of γ-Al_2O_3.[4] Although the influence of treatment time and temperature were investigated, there was no direct comparison of the degree of hydration of the metal loaded sample and the bare support.

The X-ray diffractograms and ^{27}Al MAS NMR spectra in this study indicate that the presence of metal particles results in a significant decrease of the rate of boehmite formation from γ-Al_2O_3. Specifically, the initial rates of boehmite conversion are 0.10 mol fraction·h^{-1} for γ-Al_2O_3, 0.05 mol fraction·h^{-1} for the Pt catalyst, and 0.02 mol fraction·h^{-1} for the Ni catalyst, respectively. This effect is quite significant, considering the catalysts contained only 1 wt % of Pt and Ni, respectively. On the basis of the TEM analysis of the untreated 1 wt % Pt/γ-Al_2O_3, the average metal cluster size is ∼1.0 nm (Figure 10). Assuming that the particles consist of a monolayer of metal, the average Pt particles consist of ∼13 Pt atoms (Pt atomic radius = 139 pm). At the present metal loading of 1 wt %, the Pt particles cover only ∼2% of the total surface area of γ-Al_2O_3 (BET surface area = 90 m^2/g). The same analysis of Ni/γ-alumina results in ∼23 atoms/cluster covering ∼5.5% of the available surface area. Considering that such a small fractional coverage results in a significant change in the kinetics of boehmite formation, it appears that the metal particles cover a relatively small number of specific surface sites that play a critical role in the hydration process.

The ^{1}H NMR spectra clearly show that the addition of metal particles reduces the concentration of surface hydroxyl groups (Figure S3). It is well established that the metal precursors bind to these sites during wet impregnation.[42,43] The present data indicate that the metal particles remain in these locations after calcination. Integration of the spectra indicated an 8.3% decrease in the concentration of surface OH groups for the platinum catalyst and a 31.8% decrease for the nickel catalyst, showing that the number of blocked hydroxyl groups in 1 wt % Ni/γ-Al_2O_3 is ∼3.8 times higher than in 1 wt % Pt/γ-Al_2O_3. This is in general agreement with the molar ratio of nickel/platinum atoms (3.3) in samples containing 1 wt % metal. It is interesting to note that 1.7 and 1.3 surface hydroxyl groups were consumed per nickel and platinum atom, respectively. A similar stoichiometry was reported in a study on grafting molybdates on γ-Al_2O_3 surfaces.[27]

Analysis of the ^{1}H MAS NMR spectra shows that platinum particles preferentially bind to the singly coordinated OH group

dx.doi.org/10.1021/cs1001515 |ACS Catal. 2011, 1, 552–561

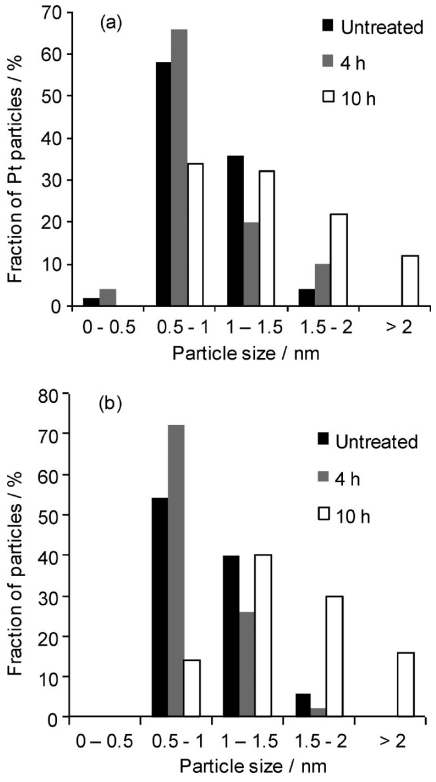

Figure 9. Metal particle histograms as measured by TEM for 1 wt % Pt/γ-Al_2O_3 (a) and 1 wt % Ni/γ-Al_2O_3 (b) for untreated and samples treated at 200 °C and vapor pressure.

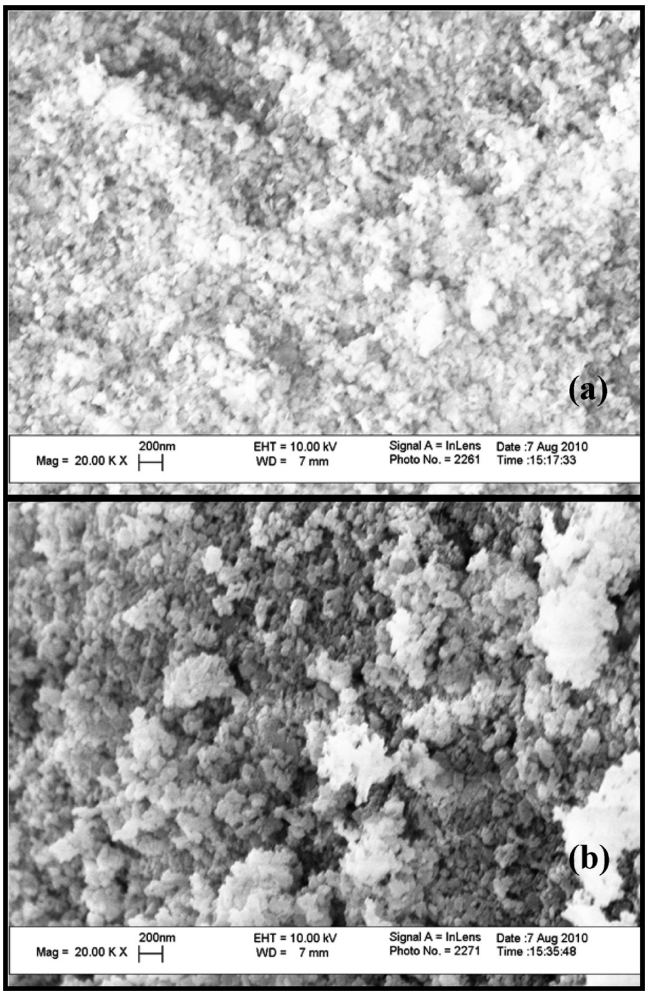

Figure 10. SEM analysis of 1 wt % Pt/γ-Al_2O_3 untreated (a) and the sample treated for 4 h (b) at 200 °C and vapor pressure.

resonating at −0.4 ppm. Incorporation of nickel particles reduced the concentration of all OH species with a slight preference for singly coordinated hydroxyl groups. Note that the singly coordinated species are the most basic surface hydroxyl groups.[44] Since the metal particles are associated with surface hydroxyl groups, we hypothesize that the decrease in the rate of hydration is caused by the decrease in concentration of these hydroxyl groups. There are two possible effects that can explain these results: (1) metal particles block sites that are important for nucleation of boehmite crystals or (2) surface-bound metal particles prevent hydration of the support.

The first mechanism seems less likely, considering that notable boehmite formation occurs even within the first hour of treatment of the metal catalysts, as shown by the ^{27}Al MAS NMR analysis. If the metal particles were blocking nucleation sites, a measurable conversion of the support would not be expected. Evidence for the second mechanism is provided by the comparison of surface area to the rate of boehmite formation. For all samples, the maximum in the surface area was observed when 23 ± 4% of the support had been converted to boehmite. The subsequent decrease in surface area was accompanied by a notable increase in the XRD peaks. This critical stage occurs significantly later when metal particles are present. Therefore, it is plausible that metal particles effectively hinder the formation of the initial boehmite patches by preventing the hydration of the alumina surface. Since the platinum and nickel catalysts exhibit comparable rates of boehmite formation and platinum shows association only with basic surface hydroxyl groups, we speculate that these OH groups may play a key role in initiating the hydration.

The chemisorption analysis and TEM indicate that metal dispersion remains constant for the first 4 h of the treatment but decreases dramatically when the treatment is extended from 4 to 10 h (Table 2). This is attributed to metal sintering. It has been shown that metal particles do not sinter on supports that are stable in hot liquid water,[15] whereas notable sintering occurs on less stable supports.[4,15] Therefore, it is suggested that sintering is triggered by erosion of the support around the metal particles.

4.3. Surface Acidity. It is well-known that the concentration and strength of acid sites have an enormous influence on the activity and selectivity of catalysts. It was reported that Brønsted acid sites can be formed by dissociative chemisorption of water on α- and γ-alumina.[44,45] Conflicting reports exist regarding the effect of recalcination of hydrated alumina. An increase in total acidity compared with the original alumina was reported,[40] whereas other researchers observe a decrease in acid site concentration of recalcined samples.[38]

In the present study, the concentration of acid sites was probed by adsorption of pyridine, followed by IR spectroscopy. This technique allows for identification of pyridine in specific environments (e.g., adsorbed on Brønsted or Lewis acid sites) and, thus, avoids the lack of specificity of surface interaction of ammonia.[46] No Brønsted acid sites were found on untreated γ-Al_2O_3 and boehmite. It was suggested previously that even the most acidic surface OH groups in γ-Al_2O_3 lack the necessary strength to protonate pyridine to form an adsorbed pyridinium

dx.doi.org/10.1021/cs1001515 |ACS Catal. 2011, 1, 552–561

Scheme 1. Dehydroxylation Sequences of Alumina Hydrates

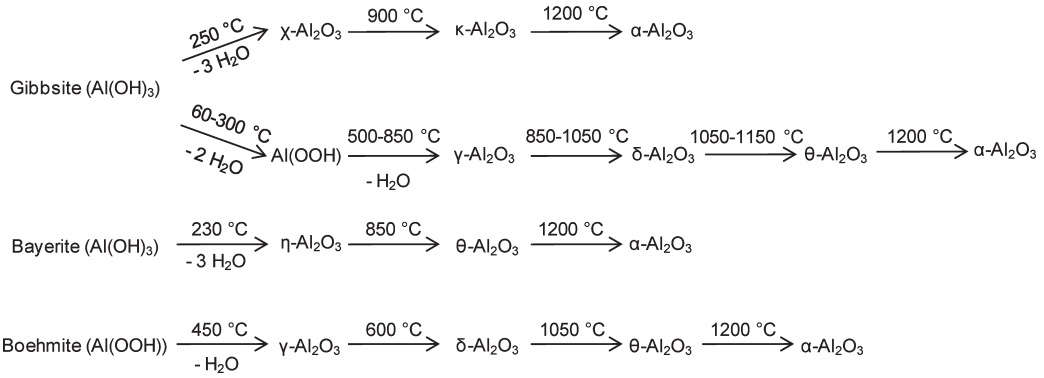

ion.[47] The present results indicate that the same is true for surface hydroxyl groups in boehmite and partially hydrated alumina samples.

A decrease in the LAS concentration as a function of treatment time was positively correlated with the fraction of γ-alumina that is converted to boehmite (Figure 6). These results are not surprising, considering the structural differences between the two materials. γ-Alumina has a defect spinel structure with aluminum cations found in both tetrahedral and octahedral coordination. Lewis acidity requires coordinatively unsaturated species, and the concentration of these sites depends on the exposed face.[48] Typically, Lewis acid sites are associated with tetrahedrally coordinated Al atoms, although they may also be generated from octahedrally coordinated Al species by desorption of nonbridging terminal hydroxyl groups.[49] During hydration, water dissociatively adsorbs on the Lewis acid sites to form boehmite, which contains only octahedrally coordinated aluminum.[45] Therefore, boehmite would be expected to have a lower concentration of Lewis acid sites.[50] It is interesting to note that the concentration of Lewis acid sites decreased linearly with increasing concentration of boehmite. This observation implies that the hydration of bulk aluminum oxide occurs at the same rate as the consumption of accessible Lewis acid sites.

The acid site analysis also revealed an increase in the LAS concentration for the untreated Pt/γ-Al_2O_3 compared with untreated γ-Al_2O_3. It is suggested that this increase arises from modifications of the surface by residual chlorine anions from the H_2PtCl_6 precursor salt. Treatment of Pt/Al_2O_3 catalyst with NH_4Cl was shown to increase the strength and concentration of Lewis acid sites on the support.[51] Adsorption of trimethylphosphine followed by ^{31}P MAS NMR spectroscopy revealed that the concentration of strong LAS increased while the concentration of weak acid sites decreased after chlorination.[52]

4.4. Relevance for Catalyst Design. The transformations observed in the present work are expected to have a significant effect on the performance of heterogeneous catalysts in aqueous phase reactions. For example, Pt/Al_2O_3 catalysts have been used for the production of hydrogen and alkanes from biomass-derived oxygenates by aqueous phase reforming.[6,9,53] Alkanes are formed via a combination of acid-catalyzed dehydration steps and metal-catalyzed hydrogenation. For production of hydrogen, C−C, C−H, and O−H bonds are cleaved on metal sites, followed by water−gas shift reaction.[6,9] As expected, the selectivity toward alkanes increases with increasing acidity of the support.[54] On the basis of the present results, it is expected that a shift in selectivity to hydrogen will occur gradually until the entire support has been converted to boehmite. However, metal sintering should also influence the activity and selectivity. It is likely that a loss in active metal surface area due to particle sintering will lower overall activity.

The presence of surface hydroxyl groups in boehmite-supported catalysts may also have synergistic effects in metal-catalyzed reactions. A recent publication reported an increased activity and selectivity for the hydrogenation of methyl propionate over RuPt/boehmite compared with RuPt/γ-Al_2O_3.[55] The authors proposed that the hydroxyl sites polarize the C═O group of the reactant, rendering it more susceptible to hydrogenation.

Regeneration of spent alumina catalysts is a possibility, but the required calcination step would likely lead to sintering of the metal particles. Additional treatments would be necessary to redisperse the metal particles. Perhaps a more desirable approach would be to alter the support in an effort to prevent hydration. The present study demonstrates that metal particles can affect hydration kinetics. It may be possible to enhance the stability of γ-Al_2O_3-supported catalysts in hot liquid water further by eliminating more of the initial hydration sites for boehmite formation. This may be achieved by capping these sites via a postsynthesis treatment. It should also be considered whether boehmite is a good support for specific catalytic reactions in aqueous phase. The use of a thermodynamically stable phase would prevent undesirable changes of the structure and properties of solid catalysts.

5. CONCLUSIONS

The present study demonstrates that significant transformations of alumina-supported catalysts occur in aqueous phase, which can strongly affect their performance in catalytic reactions. Specifically, γ-alumina is transformed into a hydrated boehmite phase with significant changes in surface area and acidity. In the initial stages of this transformation, small boehmite patches without long-range order are formed. These domains age to form compact crystalline boehmite with decreased surface area and acidity. Supported metal particles decrease the rate of the transformation of γ-alumina support to boehmite. It is proposed that associated metals hinder the initial stages of hydration and boehmite formation by effectively blocking surface hydroxyl groups important for hydration. The metal particles also exhibit sintering behavior over the course of treatment, with the most significant sintering happening after 10 h of treatment. The

dx.doi.org/10.1021/cs1001515 |ACS Catal. 2011, 1, 552–561

transformations observed here may lead to deactivation or enhanced activity for specific reactions. In either case, structural changes in aqueous environments must be considered in designing efficient catalysts for biomass reforming in aqueous media. Stabilization of alumina supports by blocking surface hydroxyl sites may be a way to design more robust catalysts for reactions in water at elevated temperature.

■ ASSOCIATED CONTENT

Supporting Information. Additional ^{27}Al MAS NMR spectra and X-ray diffractograms of the catalysts after different treatment times are provided. In addition, supplemental TEM images along with ^{1}H MAS NMR spectra of untreated samples are shown. The quantification of boehmite by ^{27}Al MAS NMR and thermogravimetric analysis is compared. This material is available free of charge via the Internet at http://pubs.acs.org.

■ AUTHOR INFORMATION

Corresponding Author

*Phone: +1-404-385-7685. Fax: +1-404-894-2866. E-mail: carsten.sievers@chbe.gatech.edu.

■ ACKNOWLEDGMENT

We thank Johannes Leisen for NMR technical support and Johannes Lercher for fruitful discussions. Access to analytical equipment from Christopher W. Jones, Sankar Nair, and Krista Walton is greatly appreciated. We acknowledge Adam Van Pelt for thermogravimetric analysis experiments. We also thank the Brook Byers Institute for Sustainable Systems, the Hightower Chair, and the Georgia Research Alliance for funding.

■ REFERENCES

(1) Yan, W.; Suppes, G. J. *J. Chem. Eng. Data* **2008**, *53*, 2033–2040.
(2) Huber, G. W. *NSF, 2008. Breaking the Chemical and Engineering Barriers to Lignocellulosic Biofuels: Next Generation Hydrocarbon Biorefineries*; National Science Foundation, Washington, DC, 2008.
(3) Ravenelle, R. M.; Schüssler, F.; D'Amico, A.; Danilina, N.; van Bokhoven, J. A.; Lercher, J. A.; Jones, C. W.; Sievers, C. *J. Phys. Chem. C* **2010**, *114*, 19582–19595.
(4) Li, H.; Xu, Y.; Gao, C.; Zhao, Y. *Catal. Today* **2010**, *158*, 475–480.
(5) Bell, A. T.; Gates, B. C.; Ray, D. *Catalysis for Energy*; DOE BES report; US Department of Energy: Washington, DC,2008.
(6) Shabaker, J. W.; Davda, R. R.; Huber, G. W.; Cortright, R. D.; Dumesic, J. A. *J. Catal.* **2003**, *215*, 344–352.
(7) Tanksale, A.; Wong, Y.; Beltramini, J. N.; Lu, G. Q. *Int. J. Hydrogen Energy* **2007**, *32*, 717–724.
(8) Shabaker, J. W.; Huber, G. W.; Davda, R. R.; Cortright, R. D.; Dumesic, J. A. *Catal. Lett.* **2003**, *88*, 1–8.
(9) Cortright, R. D.; Davda, R. R.; Dumesic, J. A. *Nature* **2002**, *418*, 964–967.
(10) Fukuoka, A.; Dhepe, P. L. *Angew. Chem., Int. Ed.* **2006**, *45*, 5161–5163.
(11) Valenzuela, M. B.; Jones, C. W.; Agrawal, P. K. *Energy Fuels* **2006**, *20*, 1744–1752.
(12) Holleman, A. F.; Wiberg, E. *Inorg. Chem.*, 34th ed.; Academic Press: New York, 2001.
(13) MacDonald, D. D.; Butler, P. *Corros. Sci.* **1973**, *13*, 259–274.
(14) Luo, N.; Fu, X.; Cao, F.; Xiao, T.; Edwards, P. P. *Fuel* **2008**, *87*, 3483–3489.
(15) Ketchie, W. C.; Maris, E. P.; Davis, R. J. *Chem. Mater.* **2007**, *19*, 3406–3411.
(16) Datka, J.; Turek, A. M.; Jehng, J. M.; Wachs, I. E. *J. Catal.* **1992**, *135*, 186–199.
(17) Benson, J. E.; Boudart, M. *J. Catal.* **1965**, *4*, 704–710.
(18) Delannay, F., Ed. *Characterization of Heterogeneous Catalysts*; Marcel Dekker: New York, 1984; Vol. 15.
(19) Wefers, K.; Misra, C. *Alcoa Technical Paper* 1987.
(20) Linsen, B. G.; Fortuin, J. M. H.; Okkerse, C.; Steggerda, J. J., Eds.; *Physical and Chemical Aspects of Adsorbents and Catalysts*; Academic Press: New York, 1970.
(21) Pecharroman, C.; Sobrados, I.; Iglesias, J. E.; Gonzalez-Carreno, T.; Sanz, J. *J. Phys. Chem. B* **1999**, *103*, 6160–6170.
(22) Urretavizcaya, G.; Cavalieri, A. L.; López, J. M. P.; Sobrados, I.; Sanz, J. *J. Mater. Synth. Process.* **1998**, *6*, 1–7.
(23) Zhou, R. S.; Snyder, R. L. *Acta Crystallogr., Sect. B: Struct. Sci.* **1991**, *47*, 617–630.
(24) John, C. S.; Alma, N. C. M.; Hays, G. R. *Appl. Catal.* **1983**, *6*, 341–346.
(25) Decanio, E. C.; Edwards, J. C.; Bruno, J. W. *J. Catal.* **1994**, *148*, 76–83.
(26) Knözinger, H.; Ratnasamy, P. *Catal. Rev.* **1978**, *17*, 31–70.
(27) Kraus, H.; Prins, R. *J. Catal.* **1996**, *164*, 260–267.
(28) Emeis, C. A. *J. Catal.* **1993**, *141*, 347–354.
(29) Kondo, J. N.; Nishitani, R.; Yoda, E.; Yokoi, T.; Tatsumi, T.; Domen, K. *Phys. Chem. Chem. Phys.* **2010**, *12*, 11576–11586.
(30) Morterra, C.; Emanuel, C.; Cerrato, G.; Magnacca, G. *J. Chem. Soc., Faraday Trans.* **1992**, *88*, 339–348.
(31) Wang, S.-L.; Johnston, C. T.; Bish, D. L.; White, J. L.; Hem, S. L. *J. Colloid Interface Sci.* **2003**, *260*, 26–35.
(32) Bartholomew, C. H.; Pannell, R. B. *J. Catal.* **1980**, *65*, 390–401.
(33) Mustard, D. G.; Bartholomew, C. H. *J. Catal.* **1981**, *67*, 186–206.
(34) Victoria, J. I.-J.; Robert, C. T. S.; Thomas, W. D.; Jennifer, C. S.; Sylvain, S. *J. Mater. Chem.* **1996**, *6*, 73–79.
(35) Kasprzyk-Hordern, B. *Adv. Colloid Interface Sci.* **2004**, *110*, 19–48.
(36) Lehnert, K.; Claus, P. *Catal. Commun.* **2008**, *9*, 2543–2546.
(37) Carrier, X.; Marceau, E.; Lambert, J.-F.; Che, M. *J. Colloid Interface Sci.* **2007**, *308*, 429–437.
(38) Rinaldi, R.; Fujiwara, F. Y.; Schuchardt, U. *Appl. Catal., A* **2006**, *315*, 44–51.
(39) Lefèvre, G.; Duc, M.; Lepeut, P.; Caplain, R.; Fédoroff, M. *Langmuir* **2002**, *18*, 7530–7537.
(40) Sanchez-Valente, J.; Bokhimi, X.; Hernandez, F. *Langmuir* **2003**, *19*, 3583–3588.
(41) Lopushan, V. I.; Kuznetsov, G. F.; Pletnev, R. N.; Kleshev, D. G. *Refract. Ind. Ceram.* **2007**, *48*, 378–382.
(42) Ertl, G., Knözinger, H., Weitkamp, J., Eds. *Preparation of Solid Catalysts*; Wiley-VCH: New York, 1999.
(43) Bourikas, K.; Kordulis, C.; Lycourghiotis, A. *Catal. Rev.—Sci. Eng.* **2006**, *48*, 363–444.
(44) Yang, X.; Sun, Z.; Wang, D.; Forsling, W. *J. Colloid Interface Sci.* **2007**, *308*, 395–404.
(45) Raybaud, P.; Digne, M.; Iftimie, R.; Wellens, W.; Euzen, P.; Toulhoat, H. *J. Catal.* **2001**, *201*, 236–246.
(46) Gorte, R. J. *Catal. Lett.* **1999**, *62*, 1–13.
(47) Morterra, C.; Magnacca, G. *Catal. Today* **1996**, *27*, 497–532.
(48) Digne, M.; Sautet, P.; Raybaud, P.; Euzen, P.; Toulhoat, H. *J. Catal.* **2002**, *211*, 1–5.
(49) Hirva, P.; Pakkanen, T. A. *Surf. Sci.* **1992**, *277*, 389–394.
(50) Men, Y.; Gnaser, H.; Ziegler, C. *Anal. Bioanal. Chem.* **2003**, *375*, 912–916.
(51) Beard, B. C.; Zhang, Z. C. *Catal. Lett.* **2002**, *82*, 1–5.
(52) Guillaume, D.; Gautier, S.; Despujol, I.; Alario, F.; Beccat, P. *Catal. Lett.* **1997**, *43*, 213–218.

(53) Huber, G. W.; Cortright, R. D.; Dumesic, J. A. *Angew. Chem., Int. Ed.* **2004**, *43*, 1549–1551.
(54) Davda, R. R.; Shabaker, J. W.; Huber, G. W.; Cortright, R. D.; Dumesic, J. A. *Appl. Catal., B* **2005**, *56*, 171–186.
(55) Zhou, Y.; Fu, H.; Zheng, X.; Li, R.; Chen, H.; Li, X. *Catal. Commun.* **2009**, *11*, 137–141.